TIDE-FREE FLOW VELOCITY AND STRAIN RATE OF CAMPBELL GLACIER TONGUE, EAST ANTARCTICA, MEASURED BY INSAR

Hoonyol Lee[1] and Hyangsun Han[2]

[1]Division of Geology and Geophysics, Kangwon National University, Republic of Korea (hoonyol@kangwon.ac.kr)
[2]Division of Polar Ocean Environment, Korea Polar Research Institute, Republic of Korea (hyangsun@kopri.re.kr)

ABSTRACT ... Measurement of strain rate of a floating glacier is critical to the investigation of detailed flow regime and crevassing mechanism of the ice. We measured the surface deformation of Campbell Glacier Tongue (CGT) in East Antarctica from the 14 COSMO–SkyMed one–day tandem differential interferometric SAR (DInSAR) image pairs obtained in 2011. The vertical tidal deflection of CGT in each DInSAR image was estimated by using the tide deflection ratio generated by the double–differential interferometric SAR technique. By removing the vertical tidal deflection from the DInSAR signals, we derived the tide–corrected ice velocity and strain rate of CGT. The crevasses in CGT formed perpendicular to the axis of the most tensile strain rate, from which we found that they were generated by the gravitational ice flow and not by the vertical tidal deflection.

KEY WORDS: strain rate, ice velocity, tide deflection ratio, DInSAR, Campbell Glacier Tongue, COSMO–SkyMed

1. INTRODUCTION

Crevasses are common features on the surface of glaciers. Crevassing of floating glaciers such as ice shelves and glacier tongues considerably influences ice calving and mass discharge (Benn et al., 2007). Crevasses on the grounded ice streams form by extending ice flow (Vaughan, 1993), while it is undeterminable whether the ice flow only contributes crevasse formation on the floating glaciers which experience tidal deflection (Rignot, 1996; Han and Lee, 2014). Therefore, understanding how crevasses on the floating glaciers form is needed to analyze ice dynamics.

Surface strain rate is primary indicator of crevasse formation (Harper et al., 1998; Young and Hyland, 2002). The surface strain rate of glaciers can be calculated from ice–velocity field. Differential interferometric synthetic aperture radar (DInSAR), a technique to measure surface deformation with sub–cm accuracy, has been widely used to map ice velocity over the glaciers (Young and Hyland, 2002; Rignot 2008; Rignot et al., 2011). For fast–flowing glaciers, the DInSAR pairs with short temporal baseline such as one–day were effectively used to map ice velocity, avoiding the temporal decorrelation of glacier surface (Joughin, 2002; Joughin et al., 2003).

The DInSAR signals over the grounded ice represent the surface deformation by gravitational flow only, while those over the floating glaciers include the vertical deflection due to ocean tide as well (Rignot, 1996). The vertical tidal deflection varies spatially over the floating glaciers, especially in the hinge zone (Han and Lee, 2014). In case of the one–day DInSAR pairs, magnitude of the vertical tidal deflection can be similar to that of daily ice–flow (Han and Lee, 2014).

The spatial variations of the vertical tidal deflection can be investigated by using tide deflection ratio defined as the ratio of the vertical tidal deflection of ice over tide height (Han and Lee, 2014). The tide deflection ratio can be determined by double–differential interferometric SAR (DDInSAR) technique that differentiates two DInSAR images by assuming constant ice–flow during the DInSAR data acquisitions (Rignot, 1996). Several studies tried to remove the magnitude in tide changes predicted by tide models from DInSAR signals over floating glaciers (Joughin et al., 2003; Scheuchl et al., 2012). However, they could not consider the spatial variation of the vertical tidal deflection in the hinge zone due to the lack of a series of DInSAR dataset to perform the DDInSAR, and thus their tidal corrections were to be imperfect.

In this study, we obtained a series of COSMO–SkyMed one–day tandem DInSAR pairs over Campbell Glacier Tongue (CGT) in East Antarctica and estimated tide deflection ratio by performing DDInSAR technique, to measure tide–corrected strain rate and investigate crevassing mechanism of CGT. Section 2 explains study area, dataset and methodology of the measurement of the tide–corrected ice velocity and strain rate of CGT. Results and discussion are presented in Section 3. Finally, Section 4 concludes this study.

2. MATERIALS AND METHODOLOGY

2.1 Study area

CGT is a seaward extension of Campbell Glacier (CG), which flows into the northern Terra Nova Bay in Ross Sea, East Antarctica. Figure 1 shows a COSMO–SkyMed SAR image over CGT obtained on 27 November 2011. The white lines represent the location of the grounding line of CGT (Han and Lee, 2014). CGT is composed of

two ice streams: one is the main stream in the east and the other is the branch stream composed of broken ice chunks in the west. Many crevasses are formed on the midstream of CG and the hinge zone of CGT (see the dotted boxes in Figure 1). Annual ice velocity of CGT was 180–270 m a^{-1} measured by the offset tracking of the COSMO–SkyMed SAR images between 2010 and 2011 (Han et al., 2013). CGT experiences the vertical tidal deflection up to 60 cm during a day (Han and Lee, 2014), in which the magnitude is similar to daily ice–flow of the glacier tongue.

2.2 Data

We used 14 one–day tandem interferometric SAR (InSAR) pairs over CGT obtained from January to November 2011 by COSMO–SkyMed satellites equipped with X–band SAR (Table 1). All SAR images were acquired in strip–map mode (3 m spatial resolution), VV–polarization, and an incidence angle of 40° in descending orbit at around 3:45 UTC. Global Digital Elevation Model (GDEM) of the Advanced Spaceborne Thermal Emission and Reflection Radiometer (Fujisada et al., 2005) was used to remove topographic phases from the one–day interferograms. The vertical accuracy of the GDEM is 20 m which is enough to remove topographic phases from the interferograms due to very short perpendicular baselines of the InSAR pairs.

Ross Sea Height–Based Tidal Inverse Model (Ross_Inv) (Padman et al., 2003), the optimum tide model in Terra Nova Bay (Han and Lee, 2014), was used to predict tide height at a centre point of the free–floating zone of CGT. The load–tide effect on the predicted tide height was corrected by TPXO6.2 Load Tide model (Egbert and Erofeeva, 2002). The inverse barometer effect (IBE) on the predicted tide height was corrected by using in situ atmospheric pressure measured by an automatic weather system installed near CGT.

2.3 Methodology

First, the one–day surface deformation over CGT in the line of sight (LOS) direction was extracted from the 14 differential interferograms. DInSAR signals over the grounded part of CG represent gravitational ice flow only, while those over CGT represent the vertical tidal deflection as well. We generated total 91 DDInSAR images from the 14 differential interferograms and extracted the vertical tidal deflection of the glacier tongue. The DDInSAR images clearly show the location of grounding line and the spatial variation of the vertical tidal deflection in the hinge zone of CGT. By the following methodology mentioned in Han and Lee (2014), we generated a map of tidal deflection ratio over CGT by the pixel–based linear regression between the DDInSAR–derived vertical tidal deflection and tidal variations during the DDInSAR observations predicted by the IBE–corrected Ross_Inv.

The flow velocity map was converted into the flow direction estimated by the offset tracking between two SAR images obtained on 25 October and 10 November 2011. To represent annual state of ice velocity, we generated the maps of the averaged one–day ice velocity and its standard deviation from the 14 tide–corrected one–day ice flows.

We calculated the flow–oriented strain rate such as longitudinal ($\dot{\varepsilon}_l$), transverse ($\dot{\varepsilon}_t$) and shear strain rate ($\dot{\varepsilon}_s$) by (Bindschadler et al., 1996)

$$\dot{\varepsilon}_l = \dot{\varepsilon}_{xx} \cos^2 \beta + 2\dot{\varepsilon}_{xy} \sin \beta \cos \beta + \dot{\varepsilon}_{yy} \sin^2 \beta$$
$$\dot{\varepsilon}_t = \dot{\varepsilon}_{xx} \sin^2 \beta - 2\dot{\varepsilon}_{xy} \sin \beta \cos \beta + \dot{\varepsilon}_{yy} \cos^2 \beta \qquad (1)$$
$$\dot{\varepsilon}_s = \left(\dot{\varepsilon}_{yy} - \dot{\varepsilon}_{xx}\right) \sin \beta \cos \beta + \dot{\varepsilon}_{xy} \left(\cos^2 \beta - \sin^2 \beta\right)$$

where $\dot{\varepsilon}_{xx}$, $\dot{\varepsilon}_{yy}$ and $\dot{\varepsilon}_{xy}$ are the strain rate with respect to the image axes x and y directions calculated from ice velocity, and β is the flow direction measured counter clockwise from the x axis.

3. RESULT AND DISCUSSION

3.1 Tide–corrected ice velocity

Figure 1(a) shows the ice velocity in the flow direction before tide correction, which was estimated from a DInSAR image. The white lines show the location of grounding line, while a white dotted line represents the seaward edge of the hinge zone of CGT. The ice velocity increases from the uppermost part of CG by ~20 cm day^{-1} to the seaward edge of CGT by ~90 cm day^{-1}. However, the ice velocity in the free–floating zone of CGT is about 1.2 times larger than that measured by the offset tracking of the same SAR dataset used in this study (Han et al., 2013). This is because the vertical tidal deflection was added to the ice flow and thus erroneous ice velocity was estimated.

The maps of the averaged ice velocity derived from the 14 tide–corrected ice flows and its standard deviation are shown in Figure 1(b) and (c), respectively. The ice velocity over the grounded part of CG is almost similar to that estimated from the tide–uncorrected ice velocity. Over the main stream of CGT, the ice velocity gradually increases from the grounding line (~52 cm day^{-1}) to the seaward edge of the hinge zone (~62 cm day^{-1}), while that is almost constant in the free–floating zone along the flow line (62~67 cm day^{-1}). The ice velocity over CGT estimated from the tide–corrected DInSAR signals is nearly the same as that measured by Han et al. (2013). Most areas of CG and the main stream of CGT show small standard deviation less than 4 cm day^{-1} (Figure 1(c)), which accounts for only 5% of the maximum ice velocity of 67 cm day^{-1} measured at the terminus of CGT.

The branch stream of CGT shows large standard deviation due to the irregular ice flow of the broken ice chunks (Han and Lee, 2014).

3.2 Tide–corrected strain rate

Maps of $\dot{\varepsilon}_l$, $\dot{\varepsilon}_t$ and $\dot{\varepsilon}_s$ over CG and CGT are shown in Figure 2(a), (b) and (c), respectively. Figure 2(d) shows the uncertainty in the $\dot{\varepsilon}_l$ which is similar to that in the $\dot{\varepsilon}_t$ and $\dot{\varepsilon}_s$. The $\dot{\varepsilon}_l$–map clearly shows the compression (the negative values) and extension (the positive values) zone of the glacier (Figure 2(a)). The grounded part of CG shows large variation in the $\dot{\varepsilon}_l$ values from -6.3×10^{-4} to 3.5×10^{-4} day^{-1} with the uncertainty of $\sim1\times10^{-4}$ day^{-1} due to the locally variation in the ice velocity along the flow lines. Over the main stream of CGT, a mean value of $\dot{\varepsilon}_l$ in the hinge zone was $2.3\times10^{-5}\pm2.8\times10^{-6}$ day^{-1} which is higher than that in the free–floating zone ($7.0\times10^{-6}\pm1.4\times10^{-6}$ day^{-1}). This represents that the ice stretches in the hinge zone due to increasing ice velocity along the flow line, more than in the free–floating zone of CGT where ice velocity is almost constant along the flow line. In the branch stream of CGT, the $\dot{\varepsilon}_l$, $\dot{\varepsilon}_t$ and $\dot{\varepsilon}_s$ values with large uncertainties vary spatially due to the random motion of the broken ice chunks (Han and Lee, 2014).

The $\dot{\varepsilon}_t$ values vary spatially over the grounded part of CG from -5.4×10^{-4} to 3.3×10^{-4} day^{-1} due to convergence (the negative values) and divergence (the positive values) of the ice flow (Bindschadler et al., 1996) (Figure 2(b)). At the midstream of CG where the longitudinal crevasses are formed, a mean value of $\dot{\varepsilon}_t$ is very large by $3.2\times10^{-4}\pm4.7\times10^{-5}$ day^{-1} due to the divergence of the ice flow by widening of the glacier width. The $\dot{\varepsilon}_t$ values are negative immediately below the longitudinal crevasse area (a mean $\dot{\varepsilon}_t$ value of $-5.2\times10^{-4}\pm6.4\times10^{-5}$ day^{-1}) because the width of the glacier becomes narrow and the ice–flow converges. The hinge zone of the main stream of CGT shows large $\dot{\varepsilon}_t$ value (a mean value of $3.0\times10^{-5}\pm5.3\times10^{-6}$ day^{-1}), especially over the longitudinal crevasse area. This is because the eastern part of CGT is grounded and experiences basal drag (Han and Lee, 2014), and thus ice velocity increases from the east to the west of the glacier tongue. In the free–floating zone of CGT, the $\dot{\varepsilon}_t$ values are very small (a mean value of $8.4\times10^{-6}\pm1.6\times10^{-6}$ day^{-1}) and few crevasses are observed due to spatially constant ice velocity.

High $\dot{\varepsilon}_s$ values of $\sim\pm4.3\times10^{-4}$ day^{-1} are observed along the sides of the grounded part of CG (Figure 2(c)), which is induced by the lateral drag at the glacial side walls

(Whillans and van der Veen, 1997). The midstream of the grounded part of CG shows high $\dot{\varepsilon}_s$ as well, due to the changes in width of the glacier (Payne et al. 2004). The $\dot{\varepsilon}_s$ values in free–floating zone of the main stream of CGT are very small (a mean value of $2.8\times10^{-6}\pm5.1\times10^{-7}$ day^{-1}) because of little lateral drag. Meanwhile, high $\dot{\varepsilon}_s$ values are calculated in the hinge zone (a mean value of $1.8\times10^{-5}\pm2.5\times10^{-6}$ day^{-1}), especially in the crevasse area by $\sim1.0\times10^{-4}$ day^{-1}. This means that the hinge zone of CGT experiences shearing by the lateral drag at the eastern part of the glacier tongue.

4. CONCLUSION

This study showed a method to measure tide–corrected strain rate of a floating glacier by using a series of COSMO–SkyMed one–day tandem DInSAR dataset for CGT, and analyzed the flow regime and crevassing mechanism of the glacier tongue. The vertical tidal deflection of CGT was estimated by multiplying the tidal variations corresponding to the DInSAR images by the DDInSAR–derived tide deflection ratio, which was removed from the DInSAR signals to extract ice velocity only. The orientation of crevasses in CGT was nearly perpendicular to the direction of the most tensile strain rate calculated from the tide–corrected ice velocity. This demonstrates that the crevasses form by ice flow in respect of the DInSAR accuracy, not by tidal deflection.

The tide correction of DInSAR signals over floating glaciers by using the DDInSAR–derived tide deflection ratio is useful for estimating accurate ice velocity and strain rate for analyzing crevasses. The tide–corrected ice velocity and strain rate will thus be of great value in a better understating of ice dynamics of floating glaciers.

REFERENCES

Benn, D. I., N. R. J. Hulton, and R. H. Mottram. 2007. "'Calving laws', 'sliding laws' and the stability of tidewater glaciers." *Annals of glaciology*, 46 (1): 123–130. doi:10.3189/172756407782871161.

Bindschadler, R., P. Vornberger, D. Blankenship, T. Scambos, and R. Jacobel. 1996. "Surface velocity and mass balance of Ice Streams D and E, West Antarctica." *Journal of Glaciology*, 42 (142): 461–475.

Egbert, G. D., and S. Y. Erofeeva. 2002. "Efficient inverse modeling of barotropic ocean tides." *Journal of*

Atmospheric and Oceanic Technology, 19 (2): 183–204. doi:10.1175/1520–0426(2002)019<0183:EIMOBO>2.0.CO;2.

Fujisada, H., G. B. Bailey, G. G. Kelly, S. Hara, and M. J. Abrams. 2005. "ASTER DEM performance." *IEEE Transactions on Geoscience and Remote Sensing,* 43 (12): 2707–2714. doi:10.1109/TGRS.2005.847924.

Han, H., and H. Lee. 2014. "Tide deflection of Campbell Glacier Tongue, Antarctica, analyzed by double–differential SAR interferometry and finite element method." *Remote Sensing of Environment,* 141: 201–213. doi:10.1016/j.rse.2013.11.002.

Han, H., J. Lee, and H. Lee. 2013. "Accuracy assessment of tide models in Terra Nova Bay, East Antarctica, for glaciological studies of DDInSAR technique." *Korean Journal of Remote Sensing,* 29 (4): 375–387. doi:10.7780/kjrs.2013.29.4.3.

Han, H., Y. Ji, and H. Lee. 2013. "Estimation of annual variation of ice extent and flow velocity of Campbell Glacier in East Antarctica using COSMO–SkyMed SAR images." *Korean Journal of Remote Sensing,* 29 (1): 45–55. doi:10.7780/kjrs.2013.29.1.5.

Harper, J. T., N. F. Humphrey, and W. T. Pfeffer. 1998. "Crevasse patterns and the strain–rate tensor: a high–resolution comparison." *Journal of Glaciology,* 44 (146): 68–76.

Joughin, I. 2002. "Ice–sheet velocity mapping: a combined interferometric and speckle–tracking approach." *Annals of Glaciology,* 34 (1): 195–201. doi:10.3189/172756402781817978.

Joughin, I., E. Rignot, C. E. Rosanova, B. K. Lucchitta, and J. Bohlander. 2003. "Timing of Recent Accelerations of Pine Island Glacier, Antarctica." *Geophysical Research Letters,* 30 (13): 1706. doi:10.1029/2003GL017609.

Padman, L., S. Erofeeva, and I. Joughin. 2003. "Tides of the Ross Sea and Ross Ice Shelf cavity." *Antarctic Science* 15 (1): 31–40. doi:10.1017/S0954102003001032.

Payne, A. J., A. Vieli, A. P. Shepherd, D. J. Wingham, and E. Rignot. 2004. "Recent dramatic thinning of largest West Antarctic ice stream triggered by oceans." *Geophysical Research Letters,* 31: L23401. doi:10.1029/2004GL021284.

Rignot, E. 1996. "Tidal motion, ice velocity and melt rate of Petermann Gletscher, Greenland, measured from radar interferometry." *Journal of Glaciology,* 42 (142): 476–485.

Rignot, E. 2008. "Changes in West Antarctic ice stream dynamics observed with ALOS PALSAR data." *Geophysical Research Letters,* 35: L12505. doi:10.1029/2008GL033365.

Rignot, E., J. Mouginot, and B. Scheuchl. 2011. "Ice flow of the Antarctic Ice Sheet." *Science,* 333 (6048): 1427–1430. doi:10.1126/science.1208336.

Scheuchl, B., J. Mouginot, and E. Rignot. 2012. "Ice velocity changes in the Ross and Ronne sectors observed using satellite radar data from 1997 and 2009." *The Cryosphere,* 6 (5): 1019–1030. doi:10.5194/tc–6–1019–2012.

Young, N. W., and G. Hyland. 2002. "Velocity and strain rates derived from InSAR analysis over the Amery Ice Shelf, East Antarctica." *Annals of Glaciology,* 34 (1): 228–234. doi:10.3189/172756402781817842.

Whillans, I. M., and C. J. van der Veen. 1997. "The role of lateral drag in the dynamics of Ice Stream B, Antarctica." *Journal of Glaciology,* 43 (144): 231–237.
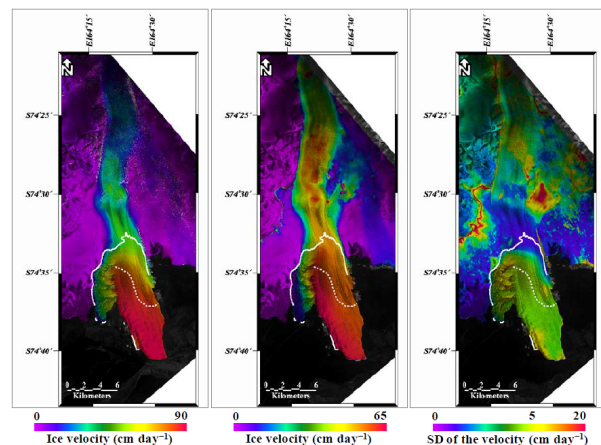
Fig. 1 Map of the ice velocity of CGT before (a) and after (b) the tide correction, its standard deviation (c) obtained from DInSAR images.
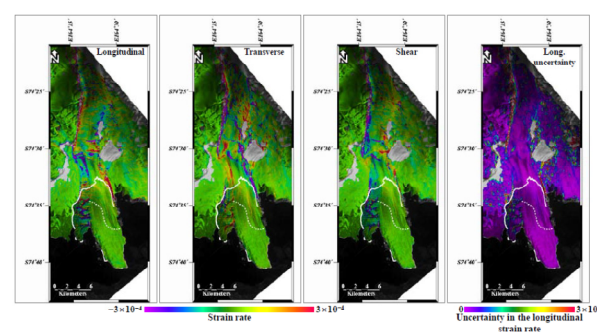

Fig. 2. Map of strain rate over CGT in (a) longitudinal, (b) transverse and (c) shear directions, respectively, while (d) is the uncertainty in the longitudinal strain rate.